~~SECRET/D~~

Marott

PERFORMANCE PREDICTION TECHNIQUES

FINAL TECHNICAL REPORT

SUBCONTRACT NO. 029B25006
DATA ITEM NO. MSM-E-108
(PAUL)

20 SEPTEMBER 1968

JAN 25 1969

~~SECRET/D~~

SECRET/D

I.   OBJECTIVES

The purpose of the Performance Prediction Techniques Study
is to develop a mathematical model that is equivalent to the PAUL
Sensor, in order to predict the sensor performance as a function
of changes in the input image characteristics or of changes in the
sensor parameters. A digital computer implementation of the model
is an objective, for the sake of an efficient and flexible predic-
tion capability.

The primary data processing element of the PAUL Sensor is a
special Sensor Tube. When this study was undertaken, it was
recognized that a realistic model would require the adequate repres-
entation of the conversion of a wide variety of input scenes into
equivalent Sensor Tube output signals. This was anticipated as an
area of greatest potential difficulty, and it received, therefore,
the major attention during this phase of the study.

II.   APPROACH

The Sensor Tube internal operations which lead to an
electrical output signal are combinations of four basic physical
phenomena. The study approach selected was to investigate these
four processes separately. A detailed mathematical representation
was first defined for each, prior to considering the interactions
which produce the output signal. These mathematical representations
are referred to as "model elements" or "elements" throughout this
report. The Sensor Tube model elements are:

1. Photoemission,
2. Electron image focusing,
3. Storage mesh surface dynamics,
4. Storage mesh transmission.

SECRET/D

SECRET/D

The physical phenomena associated with each of the above elements are random in character when individual units such as photons or electrons are concerned, but become deterministic when large numbers of units are considered together. Mathematical modeling, therefore, involves physical reasoning to define mathematical forms that describe how individual units are affected, and then prescribing appropriate mathematical operations which combine the behavior of different kinds of individual units in the proper portion and consistent with observable test behavior. These forms involve adjustable parameters, and additional parameters are required to characterize the behavior of individual tubes and the status of tube components during operation. Care must be taken to include in the model only parameters whose values can be established from laboratory measurements, or whose values can be prescribed in a given performance prediction task. The intended laboratory procedures for establishing parameter values are indicated in this report.

The processing of input scenes by the Sensor Tube is a multistage process, and additional mathematical formulations are necessary to prescribe how the model elements interact in turn to produce the tube output scene. Throughout the report, these formulations as referred to as "synthesis operations". An initial set of synthesis operations was defined during this phase of the study program, but this set has limited practical value from the standpoint of being too comprehensive for digital computation. For example, a complete description of the input scene is required; namely, the power per unit area transmitted at each wavelength at each scene point. Given the simplifications in the scene description which can be achieved by considering synthetic imagery, it appears feasible to formulate less comprehensive sets of synthesis operations, which are appropriate only to this type of imagery but

SECRET/D

SECRET/D

which can be digitally implemented. The intended route to the development of a digital computer model of the Sensor Tube is based on this concept. Evaluation of less comprehensive versions of the model against laboratory results using corresponding synthetic imagery appears feasible, and should allow verification of the model as a first step. The second step would involve the progressive sophistication of the selected synthetic imagery toward real-world imagery, and would be carried as far as is practical while maintaining digital implementation and model verification. The final step would be the representation of real-world imagery as a combination of synthetics, the effort in this direction to be concurrent with the first two steps. A section of this report titled "Synthesis Techniques" describes several types of synthetic imagery, and indicates how the corresponding simplification of the scene description allows simplifications in both the model elements and the synthesis operations.

In the following sections, the general math description of the basic tube elements is presented, the interactions which occur during each mode of the tube are described, and preliminary recommendations for synthesizing these elements into an integrated tube model are summarized.

III.   DISCUSSION OF RESULTS

A.   Introduction

In this section, the role of the Sensor Tube in the PAUL Sensor is outlined by describing the tube and by showing its relationship to the other sensor components. Following that, the four physical processes represented by the model elements are described, and related to the tube output signal. The results obtained during this phase of the program are then summarized and illustrated under separa .. adings. It should be noted that the detailed documentation of the model elements is maintained through engineering working

SECRET/D

~~SECRET/D~~

papers. Those dealing with photoemission, electron image focusing, and storage mesh transmission have been transmitted (see references). Two more, on storage mesh surface dynamics and on the comprehensive set of synthesis operations, are in preparation. An appendix is included in this report which presents the model equations associated with each of the model elements, in their most general formulation. The equations are presented in tabular form, showing the physical interpretation, method of computation, and units associated with important model quantities. A similar table for synthesis operations is presented in the section titled "Synthesis Techniques".

The PAUL Sensor receives an input optical image, detects the X,Y velocities of the image, and generates output electrical signals corresponding to the image rates. To perform these functions, the PAUL Sensor uses a special Sensor Tube in a closed electronic loop, as shown in Figure 1.

The Sensor Tube is an electro-optical device consisting of a photocathode, a deflection region, a storage element, and an output electronmultiplier section. Focusing and deflection yokes permit the photoelectron image generated by the cathode to be magnetically positioned relative to the storage surface, such that an electronic area correlation may be performed. When properly programmed through an "erase", "write", and "match" mode, this device is capable of converting an input optical image rate into a corresponding output electrical signal.

The storage element is a fine metal mesh with an insulator coating that can be electrostatically charged. Thus, an optical scene, $S(x,y)$, imaged on the photocathode generates a photoelectron image, $k_1 I(x,y)$, which generates a stored charge pattern.

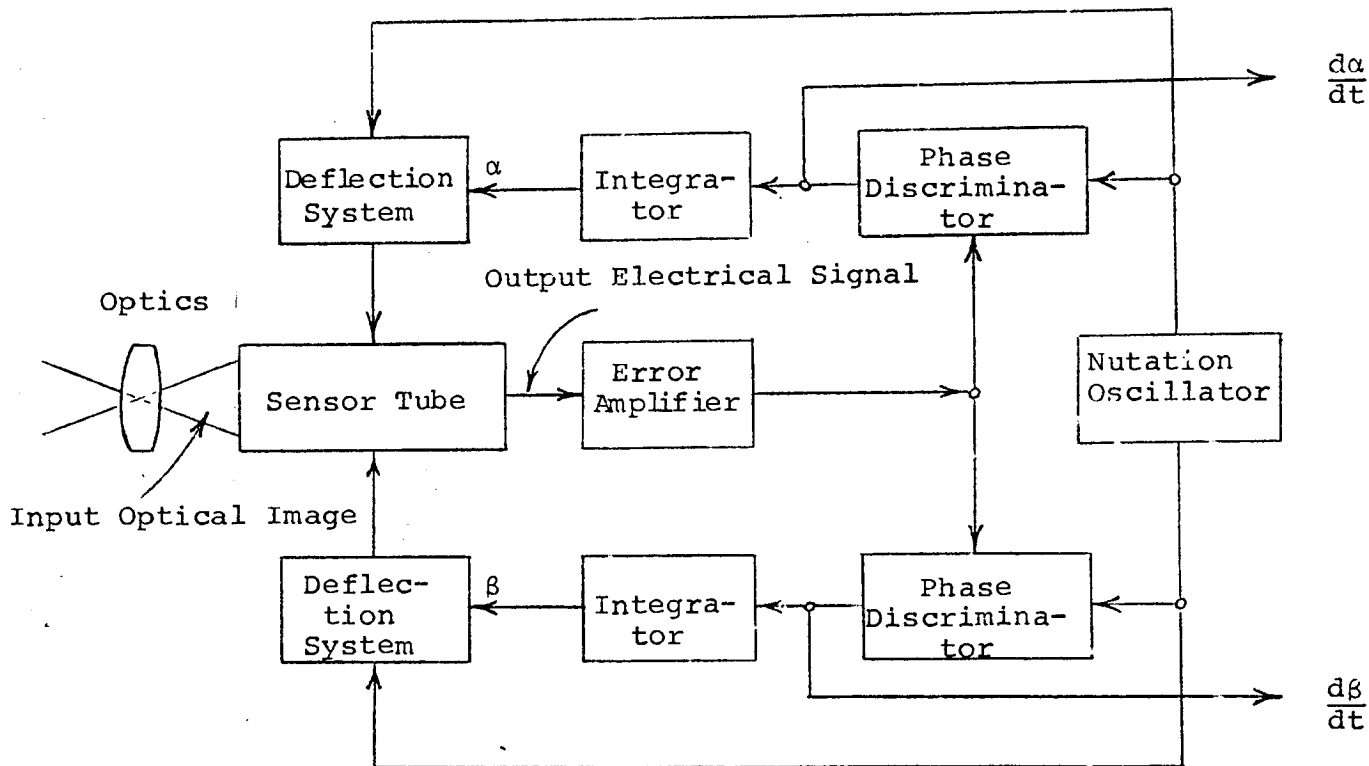$$Q(x,y) = t k_1 I(x,y) , \tag{1}$$

~~SECRET/D~~

Figure 1. PAUL Sensor Block Diagram

where k_1 is a proportionality constant dependent on the photocathode
sensitivity and spectral response, the insulator secondary emission
properties, and the transmission of the tube elements between the
photocathode and the storage element; t is the storage or exposure
time; and x and y are the coordinates of the scene referred to the

photocathode. The transmission controlling voltage pattern, $E(x,y)$, of the storage element is given by Equation (2):

$$E(x,y) = (k_2{}^{-1}) \, Q(x,y) \quad , \tag{2}$$

where k_2 is the insulator capacitance per incremental area. The controlling voltage can be modified by changing the potential of the metal mesh, which adds or subtracts by "capacitor action" a constant voltage, E_b, to the insulator surface. Thus, the transmission of the storage element, $T(x,y)$ is given by Equation (3):

$$T(x,y) = f \, [E(x,y) + E_b] \tag{3}$$

where the function is the transconductance characteristic of the storage element.

After an exposure is made, the photocathode-storage element voltage is readjusted so photoelectrons cannot strike the insulator and thus discharge the stored charge pattern. If the photocathode were uniformly illuminated, the stored voltage pattern, $E(x,y)$, would spatially modulate the uniform electron flood and generate a current charge pattern, $I_1(x,y)$, proportional to $E(x,y)$ on the side of the storage element opposite the photocathode. If instead of a uniform photocathode illumination, the same or another scene were imaged on the photocathode, the photoelectron image approaching the storage element would be $k_1 \, I_2(x,y)$, where

$$I_2(x,y) = \frac{S_2(x,y)}{k_1} \quad . \tag{4}$$

SECRET/D

The electron image at the output section now would be proportional
to $I_1(x,y)$ $I_2(x,y)$. The output section of the tube is a wide-area
electron multiplier that functions to integrate $I_1(x,y)$ $I_2(x,y)$
over the area of the storage element and to amplify the current.

The electron image can be deflected between the photocathode
and storage element. Let this deflection be α and β in the x and y
directions, respectively. With deflection, $I_2(x,y)$ becomes
$I_2(x+\alpha,y+\beta)$, and the output of the electron multiplier is the correla-
tion function, $\phi(\alpha,\beta)$, given in Equation (5):

$$\phi(\alpha,\beta) \;=\; k \int_A I_1(x,y)\; I_2(x+\alpha,\; y+\beta)\; dA \;, \qquad (5)$$

where k is the gain of the electron multiplier. This capability of
the tube to perform a simultaneous electron image correlation is
shown in Figure 2.

B.   The Model Elements

The optical input is converted to an equivalent electron
"image" in all three of the active operating modes of the Sensor
Tube. In the erase mode, an electron flood is used to bring the
storage mesh surface to a uniform potential. In the write mode,
the electron "image" corresponding to the write scene selectively
charges the storage mesh surface to produce a corresponding stored
image on that surface. In match mode, the electron image of the
match scene is selectively passed by the stored image, and con-
stitutes the current which is amplified to become the Sensor Tube
output current.

The electron images are obtained from the optical images
by the process of photoemission occurring in a thin layer of
material deposited on a glass plate (the photocathode). Viewing
this conversion as a transmission of information, the input is the

SECRET/D

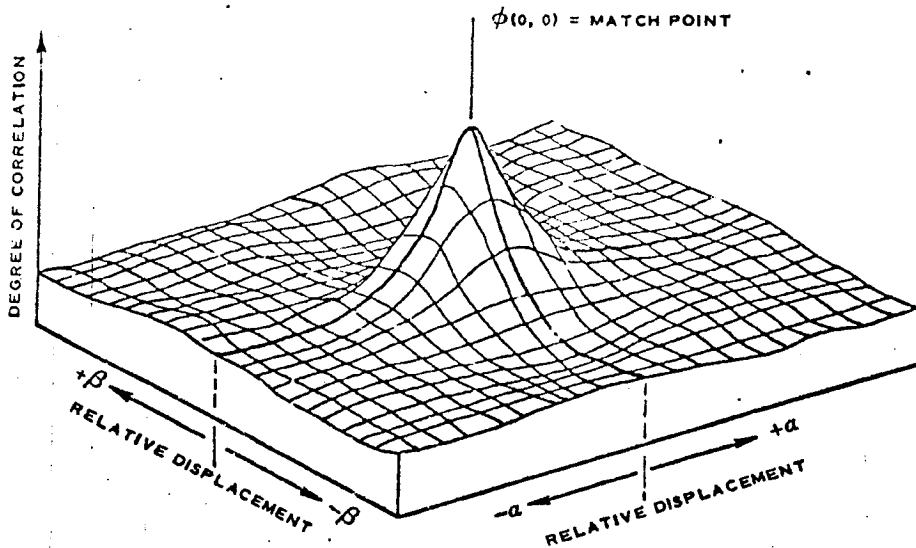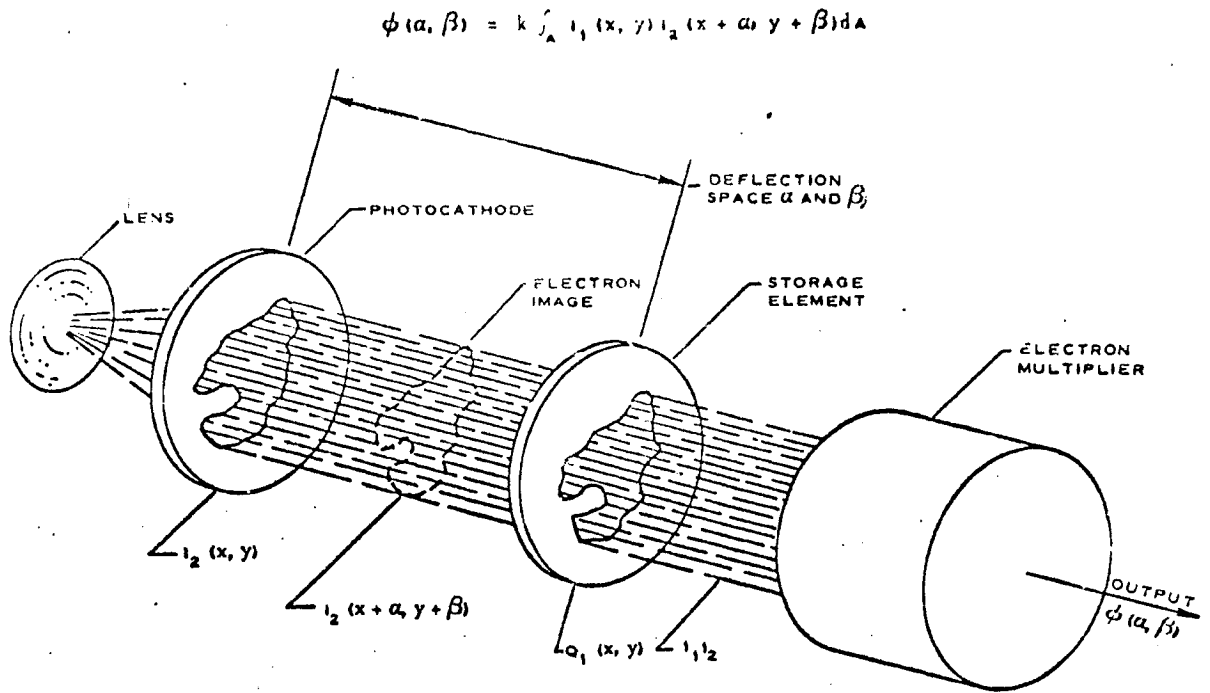$$\phi (\alpha, \beta) = k \int_A I_1 (x, y) I_2 (x + \alpha, y + \beta) dA$$

Figure 2.   Simultaneous Electron Image Correlation

color and intensity of each scene point, embodied in the power per
unit area (or number of photons per second per unit area) at each
light wavelength falling on the photocathode. The input stream of
photons at a photocathode point is partially converted to a stream
of electrons leaving the opposite side of the photocathode, moving
toward the storage mesh. The incoming photons are distinguishable
by light wavelength, but the electrons are all alike, so all the
information about the scene point that is transmitted within the
tube is embodied in the intensity of the electron stream and the
distribution of the electron velocities within the stream. That is
to say, spatial variations in the flux intensity and the velocity
distribution constitute the electron "image" of the scene. A
detailed mathematical modeling of the photoemission process was
undertaken to construct the photoemission model element, which
prescribes the flux intensity and velocity distribution resulting
from an optically focused image point on the photocathode.

Within the Sensor Tube an axially directed magnetic field
is used to keep electrons with initial transverse velocities from
flying off in all directions as they leave the photocathode. This
"focusing" magnetic field constrains electrons to spiral about a
path from a point on the photocathode to a point on the storage mesh
plane. Since the initial axial and transverse electron velocities
are distributed over ranges of values, rather than fixed at single
values, the photoelectrons cannot be completely focused at the
storage element plane, and photoelectrons emerging from a point on
the photocathode produce a pattern of current density about the
corresponding storage element plane point. These patterns are the
determining factor in the image resolution maintained in the write
and match modes. A study of how electron focusing depends on
initial electron velocity distributions, the magnetic field, and
the voltages applied to transverse mesh elements in the Sensor Tube

SECRET/D

was undertaken to obtain the <u>electron image focusing model element</u>,
which converts these variables into a point spread function des-
cribing the charge pattern at the storage mesh plane.

In the erase and write modes, the storage element surface
is exposed to photoelectrons for fixed periods of time in order to
alter the surface charge density, hence the potential of the surface.
Other factors such as the ionization of tube gases, production of
photons within the tube, field enhanced thermionic emission at the
storage element surface, and bulk leakage within the storage element
surface material, contribute to alterations in the storage mesh
surface charge density with time. Most of these factors are of
differing importance depending on the operating mode of the Sensor
Tube, and mathematical models were defined to prescribe the time-
dependent behavior of the surface charge density for each operating
mode. Taken together, these formulations constitute the <u>storage</u>
<u>mesh surface dynamics model element.</u>

The output of the Sensor Tube in the match mode is the
result of a very complex process, the variable transmission of the
match scene electron image by the storage element, as represented
earlier by Equation (5). The current density transmitted at a
storage mesh point depends on the electron image incoming at that
point, and the charge on the storage mesh about that point. The
former is prescribed by the photoemission and electron image
focusing elements, applied to the match mode conditions; the latter,
by the photoemission , the electron image focusing, and the storage
mesh surface dynamics elements, applied to the erase and write
modes in sequence.

The storage mesh transmission process was studied using
laboratory data obtained with spatially uniform erase and match
scenes, and a mathematical model was formulated which prescribes
(given a surface charge density and a number of mesh parameters)

SECRET/D

BIF-048/001- 2375-68

PAGE __12__

the fraction of an incoming electron stream of given velocity
distribution which is allowed through the storage mesh. This
formulation, which relates the results of the other model elements
to the Sensor Tube output current, is the storage mesh transmission
model element.

Results particular to each model element are described and
illustrated below, under separate headings.

The Photoemission Model Element:[1]

The yield of electron flux density from a unit photon flux
density at a given photon wavelength is well characterized by a
photocathode sensitivity characteristic $S(\lambda)$ available for particular
tubes from laboratory measurements. Integrating the product of
$S(\lambda)$ times the photon flux density at λ over all wavelengths, gives
the current density of the photoelectron image immediately. To
prescribe photoelectron velocity distributions produced by a photon
stream, however, requires a more detailed specification of the
photoemission process.

An elementary theory of photoemission was formulated for
emission from extremely thin films on the side opposite the illum-
inated side. Velocities were conveniently represented as kinetic
energies associated with the axial and transverse tube directions,
in units of electron volts. An electron was assumed to absorb the
photon energy $h\nu$ (Plank's constant times photon frequency) and to
lose a constant energy ϕ before leaving the absorption point in a
random direction. A constant work function W was assumed for the
photocathode surface on the emission side, and distribution functions
were derived for axial and kinetic energies of escaping photo-
electrons from photons of frequency ν. The distributions depended
on the parameters ϕ and W.

---

[1] M2273: "A Thin Film Theory of PAUL Sensor Tube Photoemission",
dated 10 May 1968.

SECRET/D

An expression for the photocathode yield at a given photon
wavelength was formulated, also involving ϕ and W, so that sen-
sitivity characteristics could be curve fitted to obtain reasonable
parameter values. The sensitivity characteristic of a typical tube
was fitted in the long wavelength region above 7000 $\overset{o}{A}$, to obtain the
working parameter values $\phi = -1.17$ ev, and W = 2.53 ev. At these
values, the kinetic energy distributions were shown to imply an
angular current density of emission which closely follows (at photo-
cathode-sensitive wavelengths) the Lambertian cosine law generally
accepted on the basis of experimental observations of photoemission.

Distribution functions for axial kinetic energy at a number
of light wavelengths is shown in Figure 3. The curve defines, for
a given energy in ev., the fraction of electrons having less than
that energy. At lower wavelengths, the distribution of axial
kinetic energy is indistinguishable from a uniform distribution (a
straight line) and is nearly uniform at wavelengths down to 4000 $\overset{o}{A}$.
Uniform distributions could, therefore, be adopted for mathematical
simplicity; the emission associated with a given photon frequency ν
having, as a result, an axial kinetic energy K_z uniformly distributed
from zero to

$$E(\nu) \quad = \quad h\nu - \phi - W$$

in electron volts. By the thin film theory adopted, the trans-
verse initial kinetic energy K_r along the photocathode face depends
on the axial kinetic energy by

$$K_r \quad = \quad E(\nu) - K_z \quad , \tag{6}$$

so that both axial and transverse velocity distributions are pre-
scribed by the theory adopted, for photoelectrons associated with
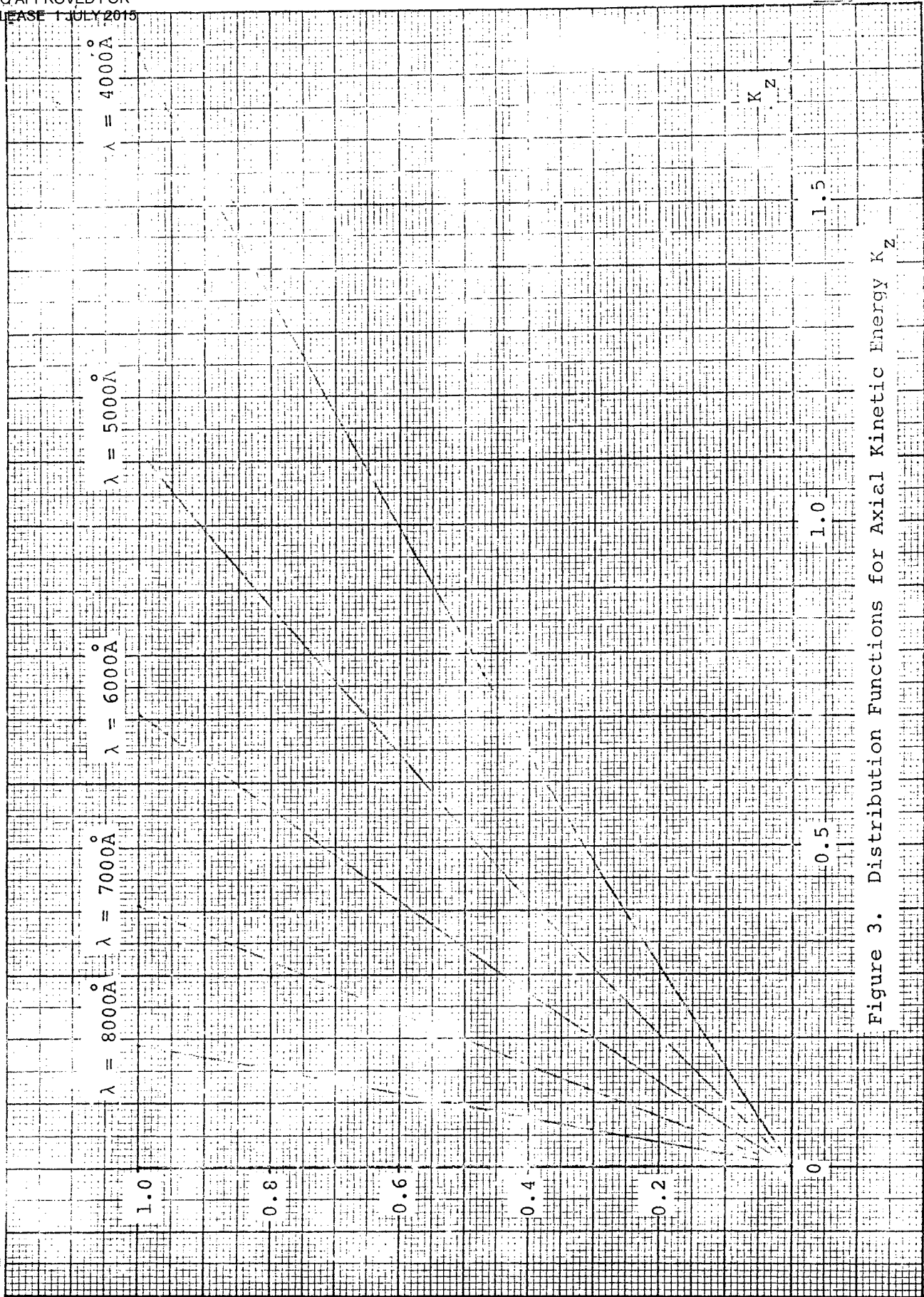photon frequency ν.

SECRET/D

Figure 3. Distribution Functions for Axial Kinetic Energy K_z

~~SECRET/D~~

The optical image point involves a mixture of photon frequencies, and the corresponding photoelectron velocity distributions can be calculated in a straightforward manner. The quantity describing the axial velocity distribution is

$$p_{K_z} (u, \bar{x}),$$

the axial kinetic energy density, which is described in the appendix.

Electron Image Focusing Model Element:[1]

The fidelity in the spatial scene variations (the resolution) which is maintained in the write and match modes of the Sensor Tube depends on the photoelectron velocity distributions, as well as the configuration and state of the tube. A study of these dependencies was made in order to derive a model element accepting these variables and returning a point spread function. The study was restricted to a state of zero deflection of the match scene, to be extended only if the model appears inadequate in simulating the spatial frequency attenuation at deflections necessary to Sensor operation.

Based on a computer-produced map of the focus magnetic field of the PAUL Sensor design, a uniform focus field was assumed. Given a magnetic field strength and the voltages applied to the transverse tube grids, then for any pair of initial axial and transverse photoelectron velocities the calculation of the point at which the electron hits the storage mesh plane is straightforward, though cumbersome. A computer program was constructed which accepts the photon wavelength λ and transverse grid voltages, and computes a quantity $R(K_z)$ defined as the distance of the λ-photoelectron landing point from that of a λ-photoelectron with no transverse initial velocity (the reference point). This quantity can be expressed as a function of the axial energy K_z alone, on the basis of the photo-

---

[1] M2273: "A Thin Film Theory of PAUL Sensor Tube Photoemission", dated 10 May 1968.

~~SECRET/D~~

~~SECRET/D~~

emission theory adopted, by which the transverse energy K_r is dependent on ν and the axial energy K_z (see Equation 6). Also by this theory, the initial transverse energy K_r is randomly oriented, so the pattern of the current density at the storage mesh plane is radially symmetric about the reference point, and is governed by $R(K_z,\lambda)$.

$R(K_z,\lambda)$, which was termed the radial spread function, prescribes the spread of current from a photocathode point for electrons associated with a single photon wavelength λ and a single axial energy K_z. Several radial spread function curves are shown in Figure 4, for a typical set of match mode transverse grid voltages.

The radial spread function is used to calculate the radial variation of the storage mesh plane current density pattern associated with a single wavelength λ, or a mixture of wavelengths. A graphical technique has been defined to obtain the radial current distribution $P(u,\lambda)$ for λ-associated photoelectrons. Mathematically, $P(u,\lambda)$ is the sum of the lengths of the intervals on the K_z scale in which $R(K_z,\lambda) < u$, divided by $E(\lambda)$. The function $P(u,\lambda)$ then represents the proportion of current within u of the reference point. This graphical technique can be replaced by a digital computer procedure for the final version of the Sensor Tube model, but it is convenient for preliminary evaluations. The method of generalization to the radial current distribution for a mixture of photon frequencies is indicated in the electron image focusing element portion of the appendix table.

Storage Mesh Surface Dynamics Element:[2]

The role of this model element is to prescribe the time dependent variations of the storage mesh surface potential during erase, write, match, and passive modes of the Sensor Tube. Different mathematical formulations are required for each mode. During

---

[2] A detailed engineering working paper is currently in preparation.

~~SECRET/D~~

SECRET/D
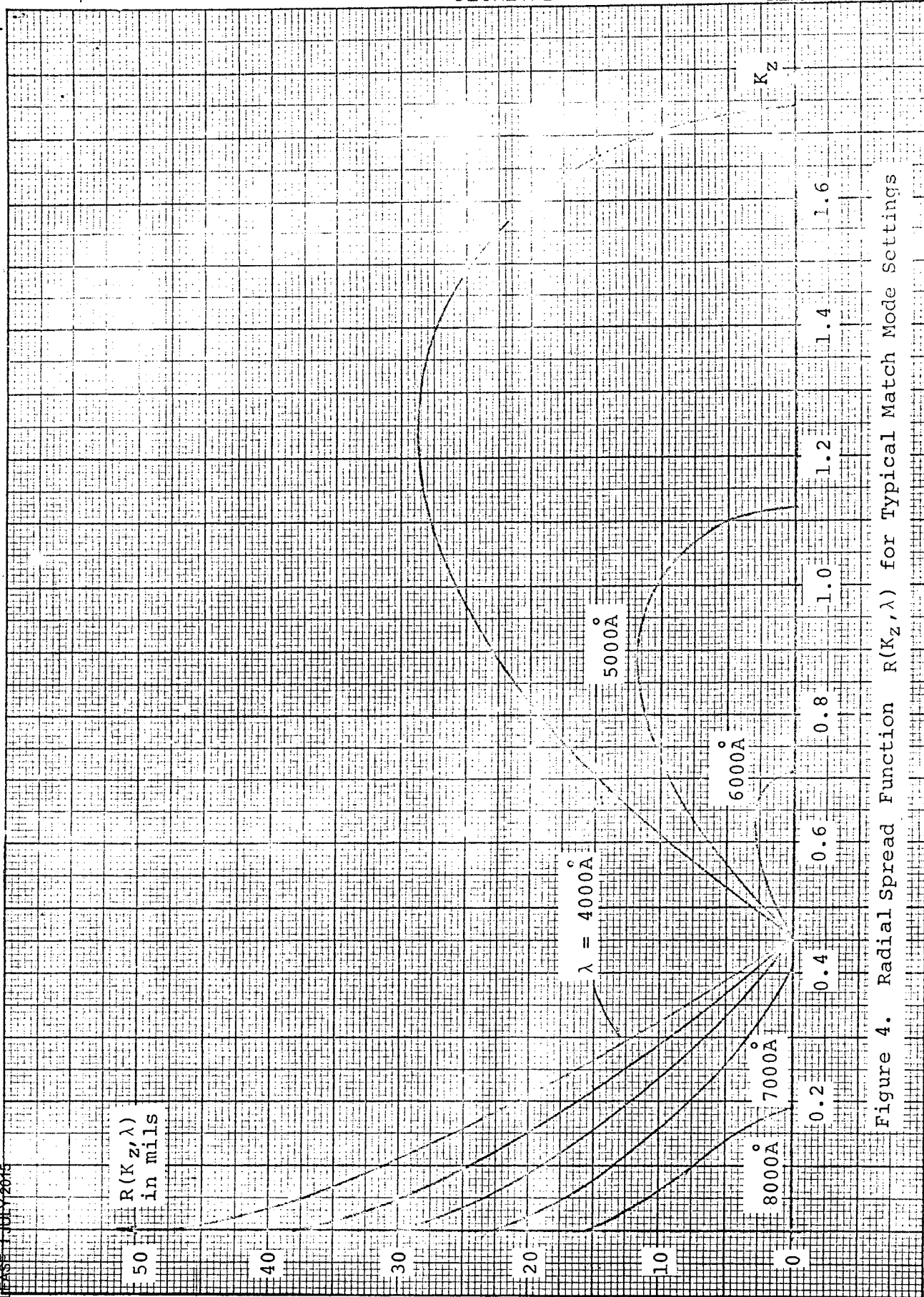
Figure 4.   Radial Spread Function $R(K_z, \lambda)$ for Typical Match Mode Settings

the erase mode, the electron image of a uniform flood of
illumination is used to cancel out positive potentials (with
respect to the photocathode) of storage mesh areas. When an area
reaches photocathode potential, however, some electrons continue to
impinge on the storage mesh by virtue of initial axial velocities,
and if the tube remains in erase, such areas are driven to a nega-
tive potential equilibrium point. The important factor in the
dynamics of this process is the emission ratio $\delta(V_s)$ prescribing
the ratio of current density out of the storage mesh surface to the
current density into the surface, as a function of the surface
potential V_s. An elementary theory was adopted to prescribe $\delta(V_s)$,
taking into account the electron axial velocity distribution as
determined by the photoemission element applied to the erase flood.
Differential equations for V_s were derived involving $\delta(V_s)$ and a
number of parameters. Although these equations have been solved
for a number of sets of parameter values, extensive comparisons
with laboratory observations remains to be done, in order to
establish and verify a set of parameters adequate to describe the
erasing process as observed in the laboratory.

Bulk leakage in the storage element is always present, and
is taken to be proportional to the potential difference between the
storage mesh surface and the potential applied to its backing wire.
Field-enhanced thermionic emission, if significant at all, can be
shown to be incorporated into this model factor. The incorporation
of the bulk leakage and the thermionic emission factor into the
differential equations for V_s in the erase mode involves only a
redefinition of parameters, and so a fit of these parameters against
observations automatically compensates for these effects during
erase. The bulk leakage-thermionic emission factor is considered
to be the only influence operating in the passive mode of the tube,
leading to a very slow exponential decay of the storage mesh
potential difference.

A constant charging rate appears applicable to the typical high voltage write mode, if ionization is ignored, in that both the initial electron velocities and the surface potential V_s are insignificant in comparison with the backing wire voltage. The correct method for incorporating the ionization has not been determined, but this is not significant at this time since the charge deposited at given write exposures can be determined experimentally, and this appears adequate for the write mode model unless anomolies become apparent.

Storage Mesh Transmission Element: [3]

The storage mesh transmission behavior was studied under conditions of uniform charge on the storage mesh surface, and uniform match scene flood. Laboratory measurements are taken under these conditions to obtain transconductance curves, which exhibit the output current as a function of the voltage applied to the fully conductive backing wire mesh of the storage element. The objective was to formulate a model of the mesh transmission which would generate transconductance curves matching those of the test data. This was achieved by mathematically fitting the laboratory curves to obtain the proper storage element model parameter values.

Based on a qualitative representation of the electric field surrounding the storage element, a mathematical form (the aperture function) was hypothesized for the transmission probability as a function of the initial axial photoelectron velocity. Combined with the distribution of the velocities supplied by the photo-emission element, the aperture function determines the fraction of incoming current that is transmitted. Thus, the aperture function characterizes the transmission behavior, and involves parameters associated with the storage element itself. By determining how the aperture function depends on the deposited charge and the backing

---

[3] BIF-048/001-2346-68: "A Uniform Flood Transmission Model", dated 8 August 1968.

mesh voltage, a computer program was constructed which generates transconductance curves, if given the tube parameters and a digital representation of the match flood color. In the model, the relationship between the parameter values and the shape and position of the generated transconductance is apparent, so the generated curves can be manipulated by trial and error to fit the laboratory curves, thus establishing parameter values.

Transconductance curves generated by using the storage mesh transmission element show good qualitative agreement with the laboratory curves in all the cases examined. Figure 5 illustrates the extent of the agreement obtained. The inset is a multiple exposure photograph showing the transconductance curves produced after erasure with the backing wire voltage set at different levels. For each curve, the horizontal scale is the backing potential during match V_b (which is increased to generate the curve) minus the backing wire potential during erase, V_{be}. For example, for the $V_{be} = 5$ curve, the cut-off of transmission occurs at about $V_b = 5$ volts and the maximum transmission occurs at about $V_b = 6.1$ volts. The drawn curves are the corresponding model curves calculated by the computer.

In order to extend the transmission model element to spatially modulated write and match scenes, it is assumed that the transmission behavior of a storage mesh point with a given charge density is the same as it would be if the entire mesh surface had the same charge density and was receiving the same current density.

C.   Synthesis Techniques

As mentioned, a set of synthesis operations (i.e., the mathematical formulations which combine the output of the model elements into a Sensor Tube model) has been derived.[4] The important quantities computed in these operations are shown in Table I.

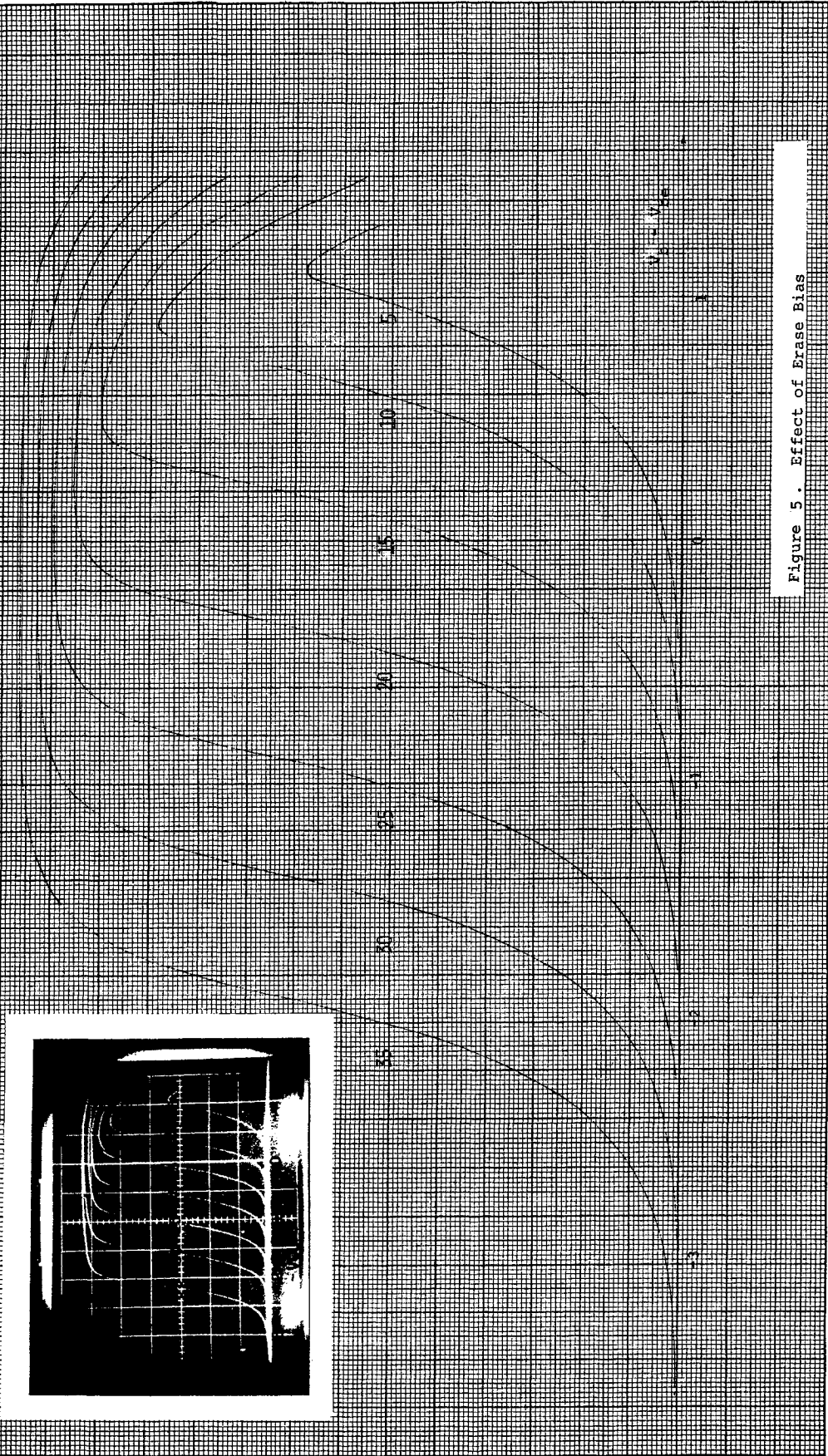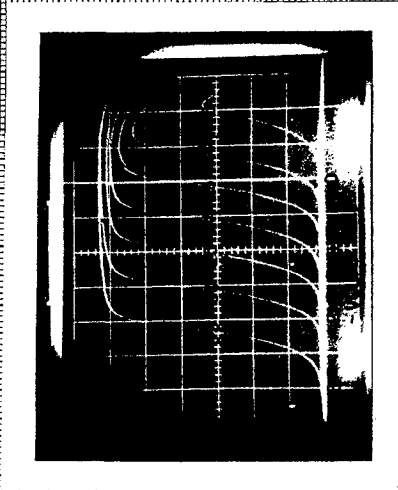[4] A detailed engineering working paper is currently in preparation.

SECRET/D

Figure 5 . . Effect of Erase Bias

SECRET/D

SECRET/D

TABLE I – SYNTHESIS OPERATIONS

Quantity	Interpretation	Determined By	Units
$\bar{V}_s$	Average mesh surface potential	$\int_{sm} V_s(\bar{y})\, d\bar{y}/s.m.\ area$	volts
$|d(\bar{x}) - \bar{y}|$	Distance from s.m. point $\bar{y}$ to a reference point (d_1, d_2)	$\sqrt{(d_1-y_1)^2 + (d_2-y_2)^2}$	cm.
$i(\bar{y})$	Incoming current density at $\bar{y}$	$\int_{pk} j(\bar{x})\, p(|d(\bar{x})-\bar{y}|,\bar{x})\, d\bar{x}$	amp cm^{-2}
$L(u, K_z, \bar{x})$	Wavelength intervals in which $R(K_z, \lambda, \bar{x}) < u$	$\{\lambda\,|\,R(K_z, \lambda, \bar{x}) < u\}$	$\overset{\circ}{A}.$
$p_{K_z}(u, \bar{y})$	Axial kinetic energy density of photoelectrons incoming at $\bar{y}$	$\frac{1}{2\pi} \int_{pk} \left[\int_0^\infty \frac{p_{K_z}(v,\bar{x})}{u} \left[\frac{d}{du} \int_{L(u)} j(\lambda,\bar{x})\, d\lambda \right] dv \right] \frac{d\bar{x}}{j(\bar{x})}$ with $u = |d(\bar{x}) - \bar{y}|$	ev^{-1}
$\phi(d)$	Output at deflection defined by $\bar{y} = d(\bar{x})$	$k \cdot \int_{sm} T(\bar{y})\, d\bar{y}$	amp

BIF-048/C01-2375-68

PAGE __23__

A physical interpretation and appropriate units are given for
each quantity. The mathematical operations seen to be necessary
to produce the quantity are indicated also by suitable expressions.
These were derived as a logical consequence of the physical inter-
pretation of quantities computed within model elements.

In the following paragraphs, some of the barriers to the
practical digital implementation of the tube model will be described,
and the necessary simplifications introduced by synthetic imagery
of several types will be indicated. From the photon frequency
spectrum of the ensemble of photons illuminating a photocathode
point, the photoemission element prescribes an axial velocity dis-
tribution of emitted photoelectrons at that point. If the photon
frequency spectrum (i.e., the "color") varies from point to point,
so does the axial kinetic energy density in the electron image.
Tracing through Table I (and appendix) would show that many essen-
tial model quantities involve integrations over the photocathode
plane of the electron axial kinetic energy density $p_{K_z}(v,\bar{x})$ times
other quantities. If this quantity varies from point to point in
a general way, digital implementations of these integrations are
both time consuming and inaccurate. For a monochromatic scene,
these integrations are eliminated entirely in some cases, or at
least simplified, since the axial kinetic energy density is the same
at each point of the photocathode, and is a constant with respect
to the integration. Monochromatic imagery is therefore a logical
simplification to make from the standpoint of digital computation.
By way of imagery sophistication, images can be considered which
consist of several areas of differing photon frequency spectrum,
for which an adjustment for the differences need be made only near
the boundaries between the areas.

A similar computation difficulty arises because of continuous
intensity variations from point to point on the photocathode. Again,

SECRET/D

area integrations over the points on which variations occur are
the difficult mathematical operations to approximate digitally.
Simplifications are apparent when intensity variations are re-
stricted to discrete intensity levels. For imagery with two levels
of intensity, for example, such an integral reduces to the weighted
sum of the two areas associated with the two intensity levels. By
systematically increasing the number of levels, compatibility with
real-world image characteristics can be approached.

The comparison of the model-generated transconductance
curves with the laboratory curves provided a sub-model verifica-
tion of the photoemission and mesh transmission elements. A sub-
model verification of the electron image focus element should also
be made using two-intensity level, monochromatic bar patterns. The
test data should be checked against the modulation transfer functions
that are computed from the model point spread function. The effect
of image deflection on the transfer functions should also be deter-
mined during this test.

The foregoing paragraphs have identified types of synthetic
imagery which can facilitate the verification of a digitally im-
plemented Sensor Tube model; verification in the sense that an
input of the physical imagery into a laboratory Sensor Tube and an
input of its mathematical description into the tube model both
produce essentially the same output signal result. Implicit in
this approach to the model development is the assumption that real
imagery may be sufficiently represented as a superposition of
synthetic imagery for which the model has been verified. To be
more explicit about this assumption, a real scene is envisioned as
(and will be presented to the final model as) a superposition of
three or more "component scenes", each monochromatic in a photon
frequency spectrum that has been incorporated into the model-
computer program. The intensity information in each of these scenes

SECRET/D

SECRET/D

will be presented to the model either as a superposition of simple quantized patterns or as a summary of the pattern characteristics. Using the write scene broken down in this way, the model program will compute a net pattern of charge on the storage mesh surface. Each "component scene" of the match scene will then be treated as if it passes the storage mesh separately, contributing its share to the output current. The process will be repeated at different displacements of the match scene with respect to the written charge pattern, to generate points which define the match curve.

IV.   RECOMMENDATIONS

It appears that a PAUL Sensor Tube model that is in the form of a digital computer program is feasible. Continuation of the model development effort should involve the construction of digital implementations of the tube synthesis operations for synthetic imagery. Verification of the model predictions and identification of the model deficiencies should be carried out, progressing from the most elementary to more complex forms for the synthetic imagery, with necessary improvements and allowable simplifications being made as required. This effort should proceed in close co-ordination with the study of the techniques for mathematically specifying[5] the input optical imagery in a form that is manageable on a digital computer.

The sensor model program, in addition to these studies, should also be expanded to include the electronics external to the tube, as required to fully describe the output signal character-istics under null and dynamic conditions, with consideration for noise and non-linear responses.

Construction and evaluation of a computer simulation program for the PAUL Sensor, incorporating the Sensor Tube model and ex-ternal electronics, will constitute the last phase of the develop-

[5]   '001-2349-68: "Image Specification Techniques - Interim Technical Report - dated 27 August 1968.

SECRET/D

SECRET/J

ment program. During this phase, actual sensor output signal
characteristics will be generated for comparison with the model
results by performing appropriate tests with the Princess Sensor
and Laboratory Simulator. In mathematically generating temporal
output signals, it should be noted that once the static match curve
characteristics have been determined for a selected pair of write
and match images, the signal data may be obtained "directly" merely
by describing the match image position as a function of time. In
order to simulate the true tracking conditions, of course, new
static match curves must be programmed as a result of periodic
changes in the input match image (line-of-sight effects) and
occasional changes in the input stored image (sensor recycle).

SECRET/D

A P P E N D I X

Table II displays the important model quantities within each model element, in approximately the order of computation from model input to model output. The physical interpretation of each quantity is given, along with any name (such as "aperture function") associated with the quantity in this report. The process of computation is indicated for each quantity in its most general mathematical formulation, and a possible choice of units is given for each quantity.

~~SECRET/D~~

TABLE II – SUMMARY OF MODEL ELEMENT QUANTITIES

Quantity	Interpretation	Determined By	Units
$\bar{x} = (x_1, x_2)$	A point on the photocathode	Definition	(cm, cm)
$\bar{y} = (y_1, y_2)$	A point on the storage mesh plane	Definition	(cm, cm)
Scene Description:			
$s(\lambda, \bar{x})$	Scene intensity spectrum (gives color and intensity at $\bar{x}$).	Model input	watts·cm⁻²·Å⁻¹
$I(\bar{x})$	Intensity at $\bar{x}$	$\displaystyle\int_0^\infty s(\lambda,\bar{x})\,d\lambda$	watts·cm⁻²
Photoemission Model Element:			
$S(\lambda, \bar{x})$	Photocathode sensitivity to λ-photons at $\bar{x}$.	Sensitivity curve or assumed sensitivity shading with $\bar{x}$	amp·watt⁻¹
$j(\lambda, \bar{x})$	Photocathode current from λ-photons at $\bar{x}$	$s(\lambda,\bar{x})\cdot S(\lambda,\bar{x})$	amp·Å⁻¹·cm⁻²
$j(\bar{x})$	Photocathode current density at $\bar{x}$	$\displaystyle\int_0^\infty j(\lambda,\bar{x})\,d\lambda$	amp·cm⁻²
$\phi(\bar{x})+w(\bar{x})$	Absorption loss plus external work function, a photo-emission parameter	$S(\phi + W, \bar{x}) = 0$	ev
$E(\lambda, \bar{x})$	Kinetic energy of λ-photoelectrons escaping photocathode at $\bar{x}$	$\dfrac{hc}{\lambda} - \phi(\bar{x}) - W(\bar{x})$	ev
$p_{K_z}(u,\lambda,\bar{x})$	Axial kinetic energy density of λ-photoelectrons escaping photocathode at $\bar{x}$	$[E(\lambda,\bar{x})]^{-1}\quad 0 < u < E(\lambda,\bar{x})$ $0\qquad$ elsewhere	ev⁻¹

~~SECRET/D~~

TABLE II – (Continued)

Quantity	Interpretation	Determined By	Units
$p_{r_z}(u,\bar{x})$	Axial kinetic energy density of electron image at $\bar{x}$	$j(\bar{x})^{-1} \int_0^{E^{-1}(u)} j(\lambda,\bar{x}) \frac{d\lambda}{E(\lambda,\bar{x})}$ where: $E^{-1}(u) = \frac{hc}{u+\phi+W}$	ev^{-1}
$K_r(\bar{x})$	Transverse kinetic energy at $\bar{x}$	$E(\lambda,\bar{x}) - K_z(\bar{x})$	ev
Electron Image Focusing:			
z_f, z_c, z_s	Distances of field mesh, collector mesh and storage mesh planes from photocathode	Tube specs.	cm
$V_f = V_c, \bar{V}_s$	Potentials of field mesh and collector mesh; average potential of storage mesh surface	V_f and V_c prescribed	volts
$\dot{z}_o, \dot{z}_f = \dot{z}_c, \dot{z}_s$	Electron velocities at pk, and field, collector and storage meshes	$\dot{z}_o = 100\sqrt{2\eta K_z}$ (K_z in ev); $\dot{z}_f = \sqrt{\dot{z}_o^2 + 2\eta V_f}$; $\dot{z}_s = \sqrt{\dot{z}_o^2 + 2\eta \bar{V}_s}$	cm sec^{-1}
t	Electron transit time from pk to storage mesh	$\frac{z_f}{\eta V_f}(\dot{z}_f - \dot{z}_o) + \frac{z_c - z_f}{\dot{z}_f} + \frac{z_s - z_c}{\eta(V_f - \bar{V}_s)}(\dot{z}_f - \dot{z}_s)$ with $\eta = 1.76\times10''$	sec
$d(\bar{x})$	Impact point on pk of $K_r=0$ electron from $\bar{x}$ – the reference point	Model input: for no deflection and no distortion $d(\bar{x}) = \bar{x}$	(cm,cm)
B	Focus field strength	Model input	gauss

TABLE II – (Continued)

Quantity	Interpretation	Determined By	Units
$R(K_z,\lambda,\bar{x})$	Radial spread function, the distance of impact point of λ-photoelectron of axial energy K_z from reference point.	$\dfrac{200}{B}\sqrt{\dfrac{2K_r}{\eta}}\left\lvert \sin\dfrac{\eta B t}{2}\right\rvert$	cm
$P(u,\lambda,\bar{x})$	Fraction of λ-current from $\bar{x}$, within u cm. of $d(\bar{x})$	$m[\psi_\lambda(u,x)]/E(\lambda,\bar{x})$ $\psi_\lambda(u,\bar{x}) = \{K_z \mid R(K_z,\lambda,\bar{x}) < u\}$ $m(\psi) = \sum$ lengths of intervals of ψ	none ev
$P(u,\bar{x})$	Fraction of current from $\bar{x}$, within u cm. of $d(\bar{x})$	$[j(\bar{x})]^{-1}\displaystyle\int_0^\infty P(u,\lambda,\bar{x})\, j(\lambda,\bar{x})\,d\lambda$	none
$p(u,\bar{x})$	Point spread function: radial density of current from $\bar{x}$ about reference point $d(\bar{x})$	$\dfrac{1}{2\pi u}\dfrac{d}{du}P(u,\bar{x})$	cm^{-2}
Storage Mesh Surface Dynamics Model Element:			
τ_b	Bulk leakage time constant	Observed decay of V_s	sec^{-1}
$V_s(t,\bar{y})$	Storage mesh surface potential in passive mode	$V_b - [V_b - V_s(0)]\,e^{-\tau_b^{-1}t}$ with $V_s(0)$ = potential at beginning of passive period	volts
$\delta_r(x)$	Fraction of electrons reflected as a function of low impact energy x at the mesh.	Assumed of form $\delta_r(x) = -\gamma_1 x + \gamma_2 x^2 \quad x > 0$ $= 0 \qquad\qquad -\varepsilon < x < 0$ $= 1 \qquad\qquad x < -\varepsilon$	none

TABLE II - (Continued)

Quantity	Determined By	Interpretation	Units
$\delta_s(x)$	Assumed of form $$\delta_s(x) = \frac{x-W}{\xi} \quad x > W$$	Emission ratio of inelastically reflected primaries, and secondaries as a function of low impact energy x	none
$\dot{\delta}(x)$	$\delta_r(x) + [1 - \delta_r(x)]\,\delta_s(x)$	Emission ratio as a function of low impact energy x at storage mesh: Ratio of current out of surface to current in.	none
$\delta(V_s, \bar{y})$	$\int_0^\infty \delta(x+V_s)p_{K_z}(x,\bar{y})\,dx$ with $p_{K_z}(x,\bar{y})$ the axial kinetic energy density for the erase flood	Emission ratio as a function of storage mesh surface potential at y	none
$\dfrac{dV_s(\bar{y})}{dt}$	$\dfrac{i(\bar{y})}{C}\,[\delta(V_s) - 1] + \tau_b(V_b - V_s)$ with C = capacitance per unit area of surface layer	Rate of change of storage mesh surface potential during erase mode at y	volt·sec^{-1}
$\sigma(V_f, V_b)$	Observed increment of Vs for given exposure (current x time), at given settings of $V_f = V_c$ and V_b.	Write constant: incorporates field mesh transmission, collector mesh transmission, emission ratio at V_b, and surface layer capacitance	cm$^2 \cdot f^{-1}$
$\Delta V_s(\bar{y})$	$\sigma \cdot i(\bar{y}) \cdot \Delta t$	Change in $V_s(\bar{y})$ during specified write exposure $i(\bar{y}) \cdot \Delta t$	volts

TABLE II – (Continued)

Quantity	Interpretation	Determined By	Units
Storage Mesh Transmission Model Element:			
w, s	Hole width, mesh spacing	Tube specs.	mil
$A_1, A_s, f, \alpha(V_s)$	Aperture function parameters	Transconductance characteristic curve fits	none
$V_\alpha(\bar{y})$	Potential of first hole-spanning. equipotential line at $\bar{y}$	$V_\alpha(\bar{y}) = \alpha V_b + (1-\alpha) V_s(\bar{y})$ $V_s(\bar{y}) =$ dielectric surface potential at $\bar{y}$	volts
$A(x,\bar{y})$	Aperture function at $\bar{y}$: fraction of $K_z = x$ current passed at $\bar{y}$	$\dfrac{A_1^2}{2A_1-A_s}\left[1-\left(\dfrac{A_1}{A_s-A_1}\right)^2 \cdot \dfrac{V_\alpha+x}{V_\alpha-V_s}\right],\ -V_\alpha < x < -V_s$ $0,\qquad x < -V_\alpha$ $A_s - \dfrac{w^2}{s^2}\, e^{-f(V_s+x)} + \dfrac{w^2}{s^2},\qquad x > -V_s$	none
$T(\bar{y})$	Density of current transmitted by mesh at $\bar{y}$	$i(\bar{y})\displaystyle\int_0 A(x,\bar{y})\cdot p_{K_z}(x,\bar{y})\,dx$ with $i(\bar{y}) =$ current density incoming at $\bar{y}$ $p_{K_z}(x,\bar{y}) =$ axial kinetic energy density of electron ensemble at $\bar{y}$	$amp\cdot cm^{-2}$